Downregulation of microRNA-4295 enhances cisplatin-induced gastric cancer cell apoptosis through the EGFR/PI3K/Akt signaling pathway by targeting LRIG1

RONG YAN*, KANG LI*, DA-WEI YUAN, HAO-NAN WANG, YONG ZHANG, CHENG-XUE DANG and KUN ZHU

Department of Oncology Surgery, The First Affiliated Hospital of Xi'an Jiaotong University, Xi'an, Shaanxi 710061, P.R. China

Received February 13, 2018; Accepted July 12, 2018

DOI: 10.3892/ijo.2018.4595

Abstract. Gastric cancer (GC) is one of the leading causes of cancer-associated mortality worldwide. The aim of the present study was to investigate the mechanism of microRNA-4295 (miR-4295), which regulates cisplatin (DDP)-induced apoptosis in GC cells through the leucine-rich repeats and immunoglobulin-like domains 1 (LRIG1)-mediated epidermal growth factor receptor (EGFR)/phosphoinositide 3-kinase (PI3K)/protein kinase B (Akt) signaling pathway. Two cell lines were selected, one with the highest expression of miR-4295 and one with the lowest expression of LRIG1, for the experiments. The half maximal inhibitory concentration of DDP in the human GC MKN-28 and MKN-45 cell lines was calculated, and mitochondrial membrane potentials of the GC cells were detected by tetramethylrhodamine, ethyl ester, perchlorate staining. The proliferation and apoptosis of GC cells with or without DDP treatment were assessed by MTT assay and plate colony formation, as well as flow cytometry and TUNEL staining. Western blot analysis and reverse transcription-quantitative polymerase chain reaction were employed to determine the expression of EGFR/PI3K/Akt signaling pathway-related genes and apoptosis-related genes. LRIG1 was identified as a target gene of miR-4295. The expression of miR-4295 was upregulated, and the expression of LRIG1 was downregulated in GC cells. Furthermore, DDP enhanced the decrease in miR-4295 expression and the increase in LRIG1 expression in GC cells. miR-4295 promoted the proliferation and inhibited the DDP-induced apoptosis of GC cells without DDP treatment. In addition, miR-4295 increased the expression levels of EGFR, PI3K, Akt, p-PI3K and p-Akt, suggesting that miR-4295 promotes the activation of the EGFR/PI3K/Akt signaling pathway by targeting LRIG1. miR-4295 targeted and negatively regulated LRIG1 expression to activate the EGFR/PI3K/Akt signaling pathway, thereby promoting the proliferation of the GC cells and inhibiting the apoptosis of the GC cells induced by DDP. Therefore, miR-4295 may be a novel therapeutic target in patients with GC.

Correspondence to: Dr Kun Zhu, Department of Oncology Surgery, The First Affiliated Hospital of Xi'an Jiaotong University, 277 Yanta West Road, Xi'an, Shaanxi 710061, P.R. China
E-mail: Drzhu_kun@163.com

*Contributed equally

Key words: microRNA-4295, gastric cancer, cisplatin, apoptosis, LRIG1, EGFR/PI3K/Akt signaling pathway,

Introduction

Gastric cancer (GC) is the most common type of cancer worldwide (1). *Helicobacter pylori* infection was reported as the initiator of the cascade and a vital factor for GC (2). There are clear differences in the incidence rates of GC in different countries. Although the incidence rate of GC has decreased, the incidence rate of gastric cardia cancer is continuing to increase in China (1,3). Despite great improvements in the clinical treatment of GC, chemotherapy remains one of the most important therapeutic strategies for the treatment of advanced GC (4). However, numerous patients eventually develop low responsiveness to chemotherapeutic drugs, including cisplatin (DDP), which may be the main cause of GC-associated mortality (5). DDP was used as a chemotherapeutic agent for treatment, and the inhibition of tumor cell proliferation was promoted by combining with DDP (6). A number of studies have documented the role of microRNAs in GC as oncogenes (7) or tumor suppressors (8), in addition to their involvement in the treatment outcomes of chemotherapy (9).

MicroRNA-4295 (miR-4295) functions as an oncogene and may be a potential biomarker for the diagnosis and treatment of bladder cancer (10). According to a cell counting kit-8 (CCK-8) proliferation assay, proliferation was promoted by miR-4295, and miR-4295 was able to promote the invasion of the ATC cell line (11). The epidermal growth factor receptor (EGFR) signaling pathway is an important transduction pathway that serves a vital role in tumor progression. The activated receptor pathway includes Ras/mitogen-activated protein kinase (MAPK), PI3K/Akt, STAT and Src family kinases, which promote the activation of transcription factors, leading to cell proliferation, invasion and migration (12). Leucine-rich repeats and immunoglobulin-like domains 1 (LRIG1) is a pan-negative regulator that is regarded as an inhibitor of the

epidermal growth factor receptor (13). The results of a study undertaken by Jiang *et al* (12) indicated that dual blockage of EGFR and its downstream PI3K/Akt signaling can act as a valuable therapeutic method to promote the anti-proliferative activity of erlotinib in pancreatic cancer (12). LRIG1 is a pan-negative regulator of the EGFR signaling pathway (13). The overexpression of miR-4295 significantly promotes the proliferation, colony formation and migration of bladder cancer cells (10). EGFR is a vital signaling component that is associated with cell growth and survival. PI3K/Akt signaling pathway activation can increase cell proliferation in tumors (14). In the present study, the targeting association between miR-4295 and LRIG1 was determined by an initial bioinformatics prediction followed by a confirmatory dual-luciferase reporter assay. The present study aimed to confirm the hypothesis that miR-4295 inhibits the apoptosis of GC cells induced by DDP via the EGFR/PI3K/Akt signaling pathway by targeting the LRIG1 gene.

Materials and methods

GEO data screening and differential expression profile analysis. The terms 'gastric cancer' and 'cisplatin' served as the key words used to search the public GEO database (http://www.ncbi.nlm.nih.gov/geo) from NCBI. The GSE31811 dataset was selected, which contained valid samples treated with DDP and invalid samples treated with DDP. The sequencing platform was GPL6480. The invalid samples treated with DDP served as controls, and differential analysis was conducted between these two datasets. The limma R package (http://master.bioconductor.org/packages/release/bioc/html/limma.html) was performed for differential analysis. $P<0.05$ and $|logFC| >2$ served as conditions to select differentially expressed genes. Next, the pheatmap package (https://cran.r-project.org/web/packages/pheatmap/index.html) of R language was adopted to construct heat maps of the differentially expressed genes.

Analyses of DDP-related genes and GC-related genes. STITCH (http://stitch.embl.de/) is a database of known and predicted interactions between chemicals and proteins. The interactions include direct (physical) and indirect (functional) associations. In this database, there were 35 differentially expressed genes associated with DDP, and the differentially expressed genes directly associated with DDP were predicted. DigSee (http://210.107.182.61/geneSearch/) is a text mining search engine that provides evidence indicating that 'genes' are involved in the development of 'disease' through 'biological events'. The term 'gastric cancer' served as the key word used to query the STITCH database. The first ten genes in the retrieval results were included in the subsequent analysis. STRING (https://string-db.org/) could retrieve the interactions between proteins. The database was used to retrieve the correlations among ten genes associated with GC in DigSee with three genes associated with DDP in STITCH.

Prediction of the microRNAs regulating LRIG1. The gene name served as the key word to retrieve the potential regulatory microRNAs of the gene in miRDB (http://www.mirdb.org/mirdb/index.html). In the miRDB TargetSearch query, the selected species was human. LRIG1 was input into the search as the gene target to retrieve the potential regulatory microRNAs of the gene in the database. The first ten microRNAs that obtained higher scores were included in the subsequent analysis. The Venn diagrams website (http://bioinformatics.psb.ugent.be/webtools/Venn/) was used to construct two Venn maps of the predicted results from two databases and to identify the intersection between the two sets of predicted results.

Cell culture, grouping and transfection. The GC MKN-28, NCI-N87, SGC-7901, MKN-45 and BGC-823 cell lines and the gastric epithelial GES-1 cell line from normal tissues (Shanghai GeneChem Co., Ltd., Shanghai, China) were cultured in RPMI-1640 medium with 10% fetal bovine serum, 100 U/ml penicillin and 100 U/ml streptomycin (Invitrogen; Thermo Fisher Scientific, Inc., Waltham, MA, USA) at 37˚C in 100% humidity and 5% CO_2. Medium was completely replaced with fresh medium every 48-72 h. The cell line with the highest expression of miR-4295 and the one with the lowest expression of LRIG1 were selected by reverse transcription-quantitative polymerase chain reaction (RT-qPCR) and western blot analysis. The MKN-45 and MKN-28 cell lines were selected, used during the logarithmic phase of growth, and classified into five groups: The blank control group (GC cells), the negative control (NC) group (pCMV-neo-Bam vector + the GC cells), the miR-4295 inhibitor group (the GC cell line + inhibitor sequence), the shRNA-LRIG1 group (the GC cells + shRNA-LRIG1), and the miR-4295 inhibitor + shRNA-LRIG1 group (co-transfection group). During transfection, the cells in the logarithmic phrase were plated into 6-well culture plates, and the density of the cells was adjusted to $2x10^5$ cells/well. The cells were transfected using Lipofectamine™ 2000 (Invitrogen; Thermo Fisher Scientific, Inc.), according to the manufacturer's protocols. A total of 8 μg plasmids (Biovector Co., Ltd., Beijing, China) and 20 μl Lipofectamine™ 2000 were dissolved with 500 μl serum-free RPMI-1640 medium without penicillin/streptomycin. Following transfection, the cells in the logarithmic phase were treated with DDP as stimulation meditation (China Institute for Food and Drug Control; batch no. 100401-201302; purity, 99.8%) at 45˚C for 45 min and further incubated in an incubator at 37˚C. After 48 h, the cell lines were used for the subsequent experiments. The blank control group and the NC group without DPP treatment were also used in the cell proliferation and apoptosis experiments.

RT-qPCR. According to the sequence in GenBank database, PCR primers were designed and synthesized (Table I) by the Shanghai GeneChem Co., Ltd. TRIzol reagent (Thermo Fisher Scientific, Inc.) was used to extract the total RNA with the one-step method, and the density and purity of the RNA were detected by ultraviolet spectrophotometer. Three micrograms of total RNA were taken and reverse transcribed by M-MLV reverse transcriptase at 37˚C for 60 min, at 99˚C for 5 min and cooled at 4˚C for 5 min. The RT-qRCR amplifications were performed using the SYBR-Green dye method (15). RT-qPCR thermocycling conditions were as follows: Pre-denaturation at 95˚C for 5 min, denaturation at 95˚C for 10 sec, annealing for 30 sec, and extension at 72˚C for 1 min. There were 40 cycles in total, followed by extension at 72˚C for 10 min. The U6 gene

was used as an internal reference of miR-4295 and β-actin was used for the other tested genes. The Cq value of each well was recorded. Each group was tested three times. Relative expression levels of reaction target genes were calculated using the $2^{-\Delta\Delta Cq}$ method (16).

Western blot analysis. The extracted protein from cells was lysed by radioimmunoprecipitation assay cell lysis buffer (Beyotime Institute of Biotechnology, Haimen, China), and the protein concentration was detected according to the manufacturer's protocol of the bicinchoninic acid Protein Quantification kit (catalog no. BCA1-1KT; Sigma-Aldrich; Merck KGaA, Darmstadt, Germany). SDS-PAGE (12%) was performed using 50 μg protein per lane. The cells were transferred to polyvinylidene difluoride membranes using the constant voltage bath method (EMD Millipore, Billerica, MA, USA). Reconstituted skimmed milk (5%) was used to block the membrane for 1 h at room temperature. Rabbit anti-human LRIG1 primary antibodies (1:1,000; catalog no. 12752), PI3K (1:1,000; catalog no. 4292), p-PI3K (1:1,000; catalog no. 13857), Akt (1:1,000; catalog no. 9272), p-Akt (1:1,000; catalog no. 9271), β-actin (1:1,000; catalog no. 4967; Cell Signaling Technology, Inc., Danvers, MA, USA), EGFR (1:1,000; catalog no. ab52894), Bcl-2 (1:500; catalog no. ab59348), Bax (1:500; catalog no. ab53154), and Caspase-3 (1:1,000; catalog no. ab90437; Abcam, Cambridge, MA, USA) were used to label the proteins on the membrane. The mixture was allowed to incubate overnight at 4˚C and was washed with TBST. Next, horseradish peroxidase-labeled goat anti-rabbit secondary antibody (1:1,000; catalog no. ab97091; Abcam) was added and incubated for 1 h at 37˚C. The mixture was washed three times with TBST for 10 min each time. An electrochemiluminescence chromogenic kit was employed to achieve chemiluminescence (Beijing Solarbio Science & Technology Co., Ltd., Beijing, China). The band density was analyzed by Quantity One software (version 4.5.2; Bio-Rad Laboratories, Inc., Hercules, CA, USA) (17).

Dual-luciferase reporter gene assay. The TargetScan (http://www.targetscan.org/vert_71/) predictions indicated that LRIG1 was the miR-4295 target gene. Luciferase reporter gene assays were used to further confirm whether LRIG1 was the target gene of miR-4295. The wild-type 3'-UTR and mutant 3'-UTR were amplified using the 3'-UTR sequence and connected with the *Xha*I locus of the pGL3 control carrier (Promega Corporation, Madison, WI, USA). The transfection reagent Lipofectamine™ 2000 was used to perform the co-transfection. The cells were allocated into four groups: LRIG1-wt 3'-UTR + miR-4295 mimic group; LRIG1-wt 3'-UTR + mimic-NC group; LRIG1-mut 3'-UTR + miR-4295 mimic group; and LRIG1-mut 3'-UTR + mimic-NC group. The culture medium was removed following co-transfection for 48 h, and cells were washed three times with PBS buffer solution. To each well of a 24-well culture plate, approximately 100 μl 1X PLB was added. The plate was gently rotated for ~15 min, and the lysate was transferred into EP tubes. The gene expression in the luciferase reporter gene assays was detected using the Dual-Luciferase assay kit (Promega Corporation), and the specific methods were conducted according to the manufacturer's protocol. The 20 μl lysate in the EP tube was transferred into the detection tube and then 100 μl LARII was added. Following mixing, firefly luciferase activity was detected, and 100 μl Stop&Glo regent was added to detect the *Renilla* luciferase activity. The results of this assay are expressed in the form of ratio of firefly luciferase activity to *Renilla* luciferase activity.

Table I. The primer sequences for reverse transcription-quantitative polymerase chain reaction.

Gene	Primer sequence
miR-4295	F: GGAAGATCTAGGATCACAGTTAACTCAGAA
	R: CGGGGTACCGCACAATCCAAAACAAGAA
LRIG1	F: ATCATCACCCAGCCAGAAAC
	R: CTACCGTGGTCCCATCCTT
EGFR	F: GAGAGGAGAACTGCCAGAA
	R: GTAGCATTTATGGAGAGTG
PI3K	F: AGGTTCATGTGCTGGATACT
	R: TGGGCTCCTTTACTAATCTC
Akt	F: ACGATGAATGAGGTGTCTGT
	R: TCTGCTACGGTGAAGTTGTT
Bcl-2	F: CGCCCTGTGGATGATGACTGAGTA
	R: GGGCCGTACAGTTCCACAAAG
Bax	F: CCCTTTTGCTTCAGGGTTTCATCCA
	R: CTTGAGACACTCGCTCAGCTTCTTG
Caspase-3	F: GACAGACAGTGGTGTTGATGATGAC
	R: GCATGGCACAAAGCGACTGGAT
U6	F: GCTTCGGCAGCACATATACTAAAAT
	R: CGCTTCACGAATTTGCGTGTCAT
β-actin	F: AGCAGAGAATGGAAAGTCAAA
	R: ATGCTGCTTACATGTCTCGAT

miR-4295, microRNA-4295; LRIG1, leucine-rich repeats and immunoglobulin-like domains 1; Akt, protein kinase B; Bcl-2, B-cell lymphoma 2; Bax, Bcl-2-associated X protein; EGFR, endothelial growth factor receptor; F, forward; R, reverse.

MTT assay. GC cells in the logarithmic growth period were collected, adjusted to a density of $8x10^4$/ml and then seeded into a 96-well plate. Two repeated wells were seeded for each group. After 1, 2, 3, 4 and 5 days, 5 g/l MTT solution (20 μl) was added to each well. The GC cells were incubated in the dark in the incubator for 4 h of culture. Next, 100 μl dimethyl sulfoxide (DMSO) was added to each well to fully agitate the crystal while avoiding light oscillation. The light absorption value (A) was detected by a microplate reader with a wavelength of 490 nm to construct the growth curve. This experiment was conducted three times, and the average value was taken. The A value in accordance with the ordinate, time (days), was taken as the abscissa for growth curve for result analysis (15).

Determination of the half maximal inhibitory concentration (IC_{50}). A total of 100 μl containing $5x10^4$/ml cells was seeded

into 96-well plates. Cells were subsequently incubated for 12 h with different concentrations of DDP (batch number: 100401-201302; 99.8%; Chinese Research Institute of Food and Drug Inspection); the DDP concentrations were 1, 2, 4, 8, 16, 32 and 64 μg/ml in 100 μl total volume per well, and three replicates were made for each concentration of the drug, using the same medium as that used in the negative control wells. Following culture for 48 h, the cells were treated with 20 μl MTT solution (5 mg/ml) in each well. After 4 h of incubation, the cell medium was removed, 150 μl DMSO was added, and cells were oscillated for 10 min. The absorbance value (A) was measured at 490 nm absorbance with automatic enzyme immunoassay. The cell growth inhibition rate (%) = (1 - A value of the experimental group/A value of the control group) x100. The IC_{50} of DDP in the human GC MKN-28 and MKN-45 cell lines was calculated.

Plate colony formation assay. The cells in the logarithmic growth phase in each group were inoculated in 6-well culture plates, and each group was seeded into 3 wells at $1x10^3$ cells/well. The 6-well plate was gently agitated in the cross direction, such that the cells would be dispersed evenly. The 6-well culture plates were incubated at 37˚C in 5% CO_2 until visible colonies were observed. The cells were carefully washed twice with PBS and fixed with 100% methanol for 15 min at 4˚C. The Giemsa staining method was used to stain the colonies for 15 min at 37˚C. The dye was slowly washed away with the water and air dried. The number of colonies that was greater than 50 was counted, and the rate of colony formation was calculated [colony formation rate = (colony number/number of inoculated cells) x100].

Annexin V-fluorescein isothiocyanate (FITC)/propidium iodide (PI) double staining. The apoptosis of the GC MKN-28 and MKN-45 cells after 24 h of cell culture was detected using the Annexin V-FITC/PI double staining kit (catalog no. 556547; Shanghai Jia Shuo Biotechnology Co., Ltd., Shanghai, China). The steps of the experiment were as follows: 10X Binding Buffer was diluted with deionized water to 1X Binding Buffer. GC cells from all groups were centrifuged at 805 x g for 5 min at room temperature, and the cells were collected. The cells were pre-cooled and then suspended in 1X PBS, centrifuged at 805 x g for 5-10 min at 4˚C, and washed. Next, 300 μl binding buffer was added to the cells. A total of 5 μl Annexin V-FITC was added. The mixture was kept in the dark and cultured for 15 min at room temperature. A total of 5 μl PI was added to the cells, and then the mixture was kept in the dark in an ice bath for 5 min immediately before using the flow cytometer (Cube6, Partec, Germany). The excitation wavelength was 480 nm, with detection of FITC at 530 nm and detection of PI at 575 nm. FlowJo software 7.6.5 (FlowJo LLC, Ashland, OR, USA) was used for analysis.

Tetramethylrhodamine, ethyl ester, perchlorate (TMRE) staining. The GC cell mitochondrial membrane potentials were detected by TMRE (Sigma-Aldrich; Merck KGaA) after all groups were cultured for 24 h. The steps of this experiment were as follows: Following treatment, the cells were seeded into 24-well plates and washed twice with preheated PBS. Next, 500 μl RPMI-1640 culture medium containing TMRE (10 nmol/l) was added to each well. The cells were incubated at 37˚C for 30 min and washed with PBS. Subsequently, 500 μl RPMI-1640 culture medium was added and detected by a fluorescence microscope (magnification, x200; Olympus Corporation, Tokyo, Japan) to count the relative fluorescence intensity.

Terminal deoxynucleotidyl transferase-mediated dUTP nick-end labeling (TUNEL) assay. The cells in the exponential phase of growth were selected and seeded into 6-well plates at a density of $1x10^8$/l for 24 h of cell culture. Three groups of cells were transfected, with two wells for each group. Following transfection for 24 h, the cells were collected and fixed with 40 g/l paraformaldehyde for 30 min at room temperature. Nick-end labeling was marked using the TUNEL method. According to the manufacturer's protocol of the Roche kit (Roche Diagnostics GmbH, Mannheim, Germany), the TUNEL staining solution was prepared with 10 μl terminal deoxynucleotidyl transferase enzyme and 240 μl fluorescent labeling agent. Next, cells were washed twice with PBS, stained with 50 μl TUNEL solution and further incubated at 37˚C for 6 min in the dark. Finally, the cells were mounted in anti-fade mounting medium after washing 3 times in PBS and were observed under a fluorescence microscope (magnification, x200). A total of 5 visual fields were randomly selected, and image analysis software Spot Advance 4.0.2 (Diagnostic Instruments, Inc., Sterling Heights, MI, USA) was used to collect images. At least 1,000 cells were counted to determine the staining results, and the apoptosis index (AI) was calculated. AI (%) = the number of apoptotic cells/1,000 cells x100 measured under an inverted microscope (magnification, x200).

Statistical analysis. All data were analyzed using SPSS 21.0 (IBM Corp., Armonk, NY, USA). Measurement data are expressed as the mean ± standard deviation. Comparisons between two groups were detected using Student's t-test. Comparisons among multiple groups were analyzed by one-way analysis of variance (ANOVA) or Kruskal-Wallis test. Data normality was checked using the Kolmogorov-Smirnov test. Comparisons among multiple groups of data with normal distribution were performed using Tukey's test for multiple comparisons in one-way ANOVA for post hoc tests, while comparisons among multiple groups of data with skewed data were performed using Dunn's test for multiple comparisons in the Kruskal-Wallis test. Comparisons of cell proliferation among groups were determined by repeated measurement ANOVA. $P<0.05$ was considered to indicate a statistically significant difference.

Results

Profile analysis of DDP sensitivity-related genes and regulatory microRNA prediction. Differential analysis was conducted between valid and invalid effective samples with DDP in the GSE31811 dataset, which revealed that there were 128 differentially expressed genes. Furthermore, 82 genes were upregulated and 46 genes were downregulated in the valid effective samples treated with DDP. Heat maps of the first 35 of the 128 differentially expressed genes were generated (Fig. 1A). For further screening the potential genes

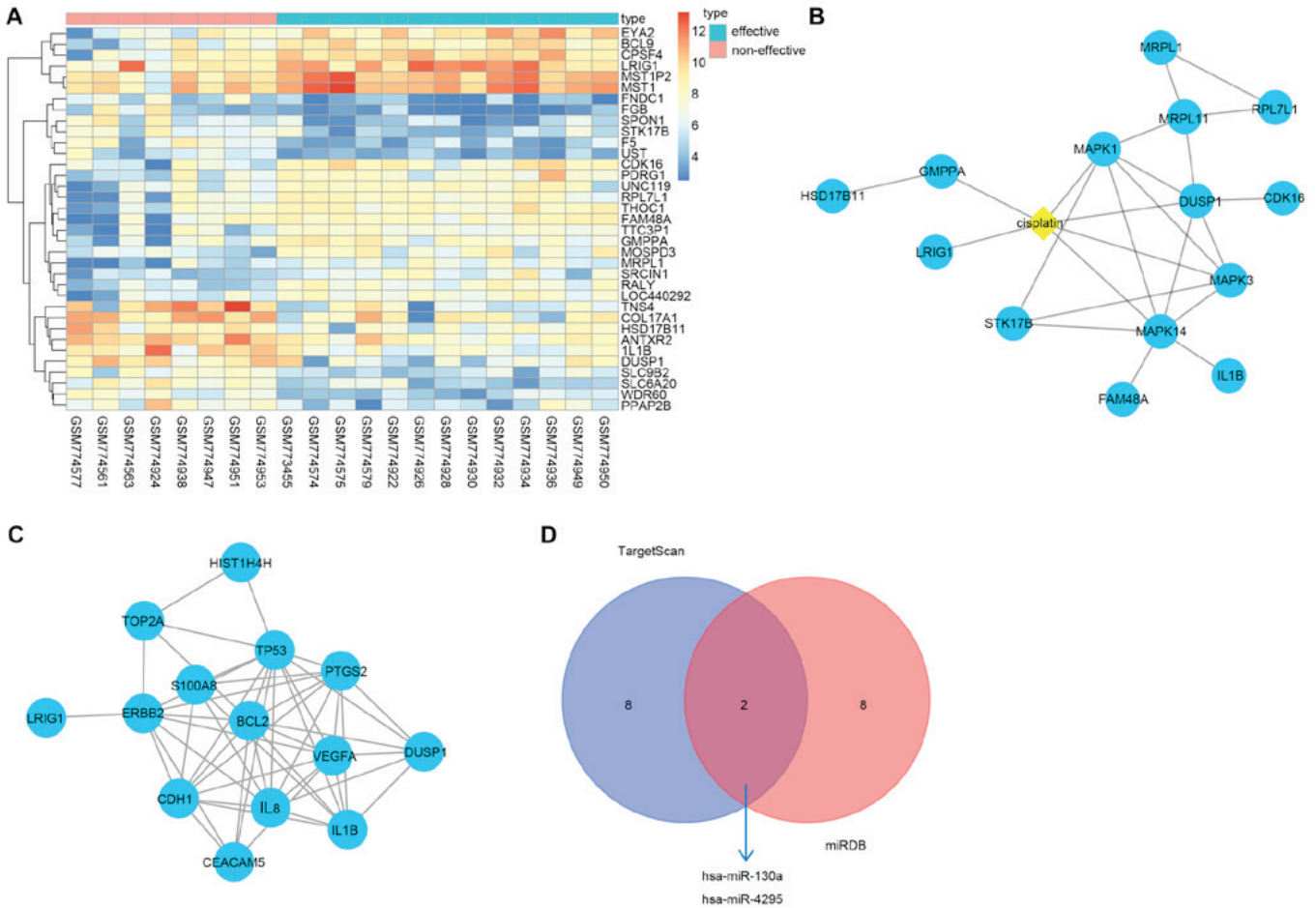

Figure 1. Expression profile analysis indicates that miR-4295 affects the sensitivity of GC cells to DDP via the PI3K/Akt signaling pathway by targeting LRIG1. Panel A, differential analysis of GSE31811. The abscissa refers to the sample number, and the ordinate refers to the differentially expressed genes. The upper right histogram presents color gradation, and the change of color from top to the bottom represents the expression of chip date changing from high to poor. Each rectangle represents the expression of each sample. Each column shows the expression of all genes in each sample. The left dendrogram refers to the cluster analysis of different genes from different samples. The horizontal stripe at the top represents the types of sample, blue represents valid samples with DDP, and red represents invalid samples with DDP. Panel B, correlations of differentially expressed genes with DDP. The yellow diamond in the center refers to DDP, the blue circle refers to genes, and the black lines refer to correlations of genes with genes and genes with DDP. The thickness of the line refers to the reliability; the thicker the line, the higher the reliability. Panel C, interactions between genes. The blue circle refers to names of genes, and the black lines refer to interactions between genes. The thickness of the line refers to the reliability; the thicker the line, the higher the reliability. Panel D, the intersection of the predicted results in the TargetScan database and the miRDB database. The left blue circle refers to the first ten microRNAs in the TargetScan database, and the right red circle refers to the first ten microRNAs that obtained higher scores in the miRDB databases; the red part in the middle refers to the intersection of predicted results in the TargetScan database and the miRDB database. miR, microRNA; GC, gastric cancer; DDP, cisplatin; PI3K, phosphoinositide 3-kinase; Akt, protein kinase B; LRIG1, leucine-rich repeats and immunoglobulin-like domains 1.

associated with DDP, the STITCH database was used to retrieve genes associated with DDP, and the 35 differentially expressed genes and DDP were analyzed in the STITCH database (Fig. 1B). The results indicated that of the 35 differentially expressed genes, LRIG1, GMPPA and DUSP1 were directly associated with DDP. These three genes were selected for further study. The genes associated with GC were retrieved, and the first ten genes in the retrieved results were included in the analysis. In the STRING database, the three differentially expressed genes and ten genes associated with GC were investigated for protein-protein interactions. The results revealed that LRIG1 interacted with ERBB2, and DUSP1 interacted with the majority of the genes in GC (Fig. 1C). To further determine the correlations between LRIG1 or DUSP1 and DDP through literature retrieval, numerous previous studies indicated that DUSP1 clearly inhibited the effectiveness of DDP. The inhibitory effects of DUSP1 on DDP were identified in a number of human cancer types, including non-small cell lung cancer (18) and ovarian cancer (19). Furthermore, the mechanisms of DUSP1 in tumors have been reported previously (20,21). In addition, a previous study reported that LRIG1 enhanced the sensitivity of cancer cells to DDP (22). All these results demonstrated that the two genes screened using the aforementioned methods were associated with the sensitivity of tumors to DDP, and LRIG1 could enhance the sensitivity of cancer cells to DDP. However, the specific mechanisms of LRIG1 have not been investigated, and the correlation between LRIG1 and DDP has also not been reported. Through further analysis of the association between DDP and GC, DDP could induce GC cell death via the PI3K/Akt signaling pathway (23,24), suggesting that LRIG1 promotion of the sensitivity of cancer cells to DDP may be achieved through the PI3K/Akt signaling pathway. To further understand the mechanisms of the effects of LRIG1 on the sensitivity of cancer

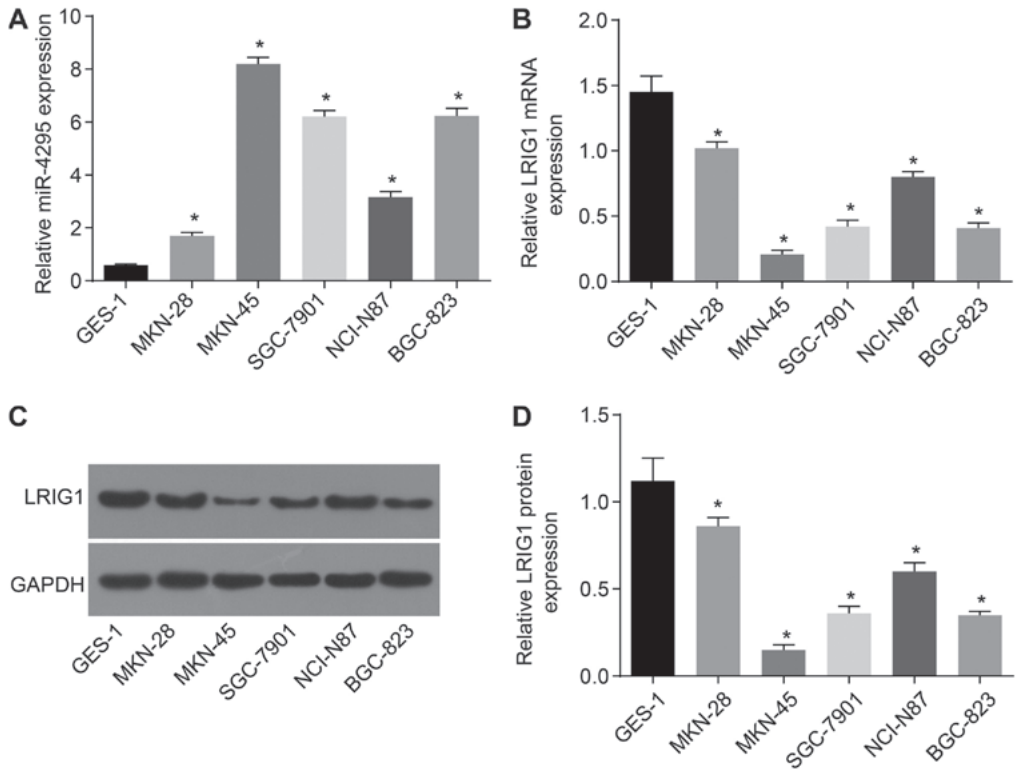

Figure 2. MKN-28 and MKN-45 GC cell lines were selected following RT-qPCR and western blot analysis. Panel A, the expression level of miR-4295 in each cell line. Panel B, the expression level of LRIG1 mRNA in each cell line. Panel C, the protein bands of LRIG1 in each cell line. Panel D, the protein levels of LRIG1 in each cell line. *P<0.01 vs. the GES-1 cell line; data are presented as the mean ± standard deviation of three independent experiments. One-way analysis of variance was used to analyze the data. RT-qPCR, reverse transcription-quantitative polymerase chain reaction; LRIG1, leucine-rich repeats and immunoglobulin-like domains 1; GC, gastric cancer.

cells to DDP, the microRNA database was used to retrieve the microRNAs that regulate LRIG1. The miRDB and TargetScan databases were used to retrieve the microRNAs that regulate LRIG1. Finally, 101 microRNAs were identified in the miRDB database, and 47 microRNAs with conserved sites were identified in the TargetScan database. The intersection of the first ten microRNAs that obtained higher scores in two databases was selected. The results demonstrated that has-miR-130a and has-miR-4295 existed in two databases (Fig. 1D). Through further analysis of the correlations between two microRNAs and DDP, previous studies have reported that miR-130a could enhance the resistance of tumor cells to DDP (25-27), while the association between has-miR-4295 and DDP has not been investigated. Therefore, has-miR-4295 was selected for further study. The aforementioned results suggested that in GC, has-miR-4295 could regulate LRIG1 expression and affect the sensitivity of GC cells to DDP via the PI3K/Akt signaling pathway.

Cell line screening for highly expressed miR-4295 and poorly expressed LRIG1 in GC. Compared with the gastric epithelial GES-1 cell line from normal subjects, the expression of miR-4295 was significantly increased in the GC cell line, while the expression of LRIG1 was significantly decreased (both P<0.05; Fig. 2). This result demonstrates that miR-4295 was overexpressed in the GC cells, and LRIG1 expression was at moderate and low levels in GC cells. Among the five GC cell lines, the expression of LRIG1 was highest in the MKN-28 cells, and the expression of miR-4295 was the lowest (all P<0.05). The MKN-45 cells presented the lowest level of LRIG1 and the highest level of miR-4295 (both P<0.05). Therefore, MKN-28 and MKN-45 cells were selected for the subsequent experiments.

LRIG1 is the downstream target gene of miR-4295. A dual-luciferase reporter gene assay was used to further confirm whether LRIG1 is the target gene of miR-4295. Results from the TargetScan website (Fig. 3A) demonstrated that LRIG1 was a target gene of miR-4295. The dual-luciferase reporter assay further confirmed this (Fig. 3B). Compared with the miR-4295 and mimic LRIG1-mut 3'-UTR co-transfection group, luciferase activity was decreased in the miR-4295 mimic and LRIG1-wt 3'-UTR co-transfection group (P<0.05). The results indicated that miR-4295 exhibited specific binding with the LRIG1 gene, and a target association existed between miR-4295 and LRIG1.

Identification of the inducing concentration of DDP in MKN-28 and MKN-45 cell lines. As demonstrated in Fig. 4, with the increase in the concentration of DDP, the inhibition rate for the MKN-28 and MKN-45 cells was increased. When the concentration of DDP was 5.84 or 25.49 μg/ml, the inhibition rate was nearly half for MKN-28 and MKN-45 cells, respectively. Therefore, the IC_{50} of DDP was 5.84 μg/ml for MKN-28 cells and 25.49 μg/ml for MKN-45 cells.

DDP reduces miR-4295 expression and increases LRIG1 expression in GC cells. RT-qPCR and western blot analysis

A

	Predicted consequential pairing of target region (top) and miRNA (bottom)	Site type	Context ++ score	Context ++ score percentile	Weighted context ++ score	Conserved branch length	PCT
Position 1066-1072 of LRIGI 3' UTR	5' ....GGUUCUGGGUAUAAUUUGCACUU...	7mer-m8	-0.25	94	-0.25	5.328	0.80
hsa-miR-4295	3' UUCCUUUUGUAACGUGAC						

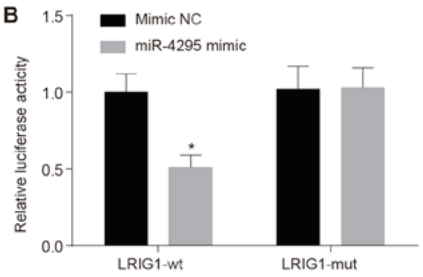

Figure 3. Targeting association between miR-4295 and the LRIG1 gene determined by an initial bioinformatics prediction followed by a confirmatory dual-luciferase reporter assay. Panel A, the results of TargetScan indicating the targeting association between miR-4295 and LRIG1. Panel B, the results of the dual-luciferase assay showing relative luciferase activity. *P<0.05 vs. the plasmid in the miR-4295 mimic and LRIG1-wt co-transfection groups. Data are presented as the mean ± standard deviation of three independent experiments. Two-tailed Student's t-tests were performed to analyze the data. miR, microRNA; LRIG1, leucine-rich repeats and immunoglobulin-like domains 1.

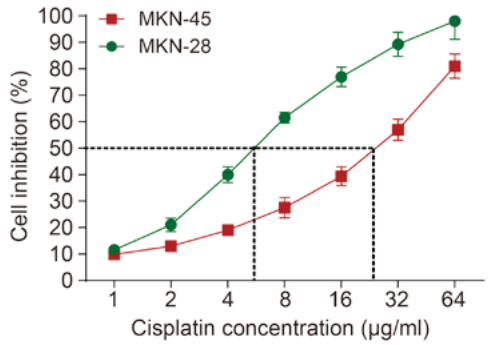

Figure 4. IC_{50} values of DDP against GC cells. GC, gastric cancer; DDP, cisplatin.

were used to measure the expression levels of LRIG1 and miR-4295 in MKN-28 and MKN-45 cells following DDP treatment. The RT-qPCR (Fig. 5) and western blot analysis results proved that following treatment with DDP, the expression level of miR-4295 was significantly decreased in MKN-28 and MKN-45 cells, and the protein and mRNA levels of LRIG1 were significantly increased (P<0.05).

miR-4295 promotes GC cell proliferation. MTT assay was used to detect the proliferation of the MKN-28 and MKN-45 GC cell lines. As demonstrated in Fig. 6A, GC cell proliferation was significantly inhibited following DDP treatment compared with cells without DDP treatment (P<0.05). Following DDP treatment, compared with the blank control group, the apoptosis of GC cells exhibited no statistically significant differences between the NC group and the miR-4295 inhibitor + shRNA-LRIG1 co-transfection group (both P>0.05). Apoptosis in the shRNA-LRIG1 group was significantly higher (P<0.05), and apoptosis in the miR-4295 inhibitor group was significantly lower (P<0.05). The results of the plate colony formation assay (Fig. 6B and C) indicated that the number of cell colonies formed in GC cells was significantly decreased, and the colony formation rate was significantly lower (P<0.05) following DDP treatment than without DDP treatment (P<0.05). Following DDP treatment, compared with the blank control group, the number of cell colonies formed in the GC cells was increased in the shRNA-LRIG1 group (P<0.05). The cell colony formation rate was significantly increased (P<0.05). The number of stained cells was significantly lower in the miR-4295 inhibitor group, which was visible to the naked eye, and the colony formation rate was significantly decreased (P<0.05). There was no statistically significant difference in the miR-4295 inhibitor + shRNA-LRIG1 co-transfection group, and the results revealed that miR-4295 and LRIG1 had antagonistic effects. The results of the plate colony formation experiment and MTT assays demonstrated that miR-4295 promoted the growth and proliferation of GC cells.

miR-4295 inhibits the DDP-induced apoptosis of GC cells. TUNEL staining was used to detect the apoptosis of GC cells. The results of Annexin V-FITC/PI double staining in Fig. 7A demonstrated that the GC cell apoptosis rate was significantly higher with DDP treatment than without DDP treatment (P<0.05). Following DDP treatment, compared with the blank control group and the NC group, the apoptosis rate of GC cells in the inhibitor group was significantly increased (P<0.05), while the apoptosis rate in the shRNA-LRIG1 group was significantly decreased (P<0.05). There was no statistically significant difference in the co-transfection group (P>0.05). The results of TUNEL staining (Fig. 7B) indicated that green fluorescence signal intensity was significantly enhanced, and apoptosis was significantly increased following DDP treatment compared with cells without DDP treatment (P<0.05). Following DDP treatment, compared with the blank group, there was no significant difference in the green fluorescence signal intensity and apoptosis in the NC group. The green fluorescence signal intensity was significantly increased in the miR-4295 inhibitor group, and cell apoptosis was also significantly increased (P<0.05), indicating that miR-4295 could inhibit the apoptosis of GC cells induced by DDP. Following LRIG1-silencing, the green fluorescence signal intensity was significantly decreased, and the apoptosis of cells was also decreased, which proved that LRIG1 could promote the DDP-induced apoptosis of GC cells. There was no

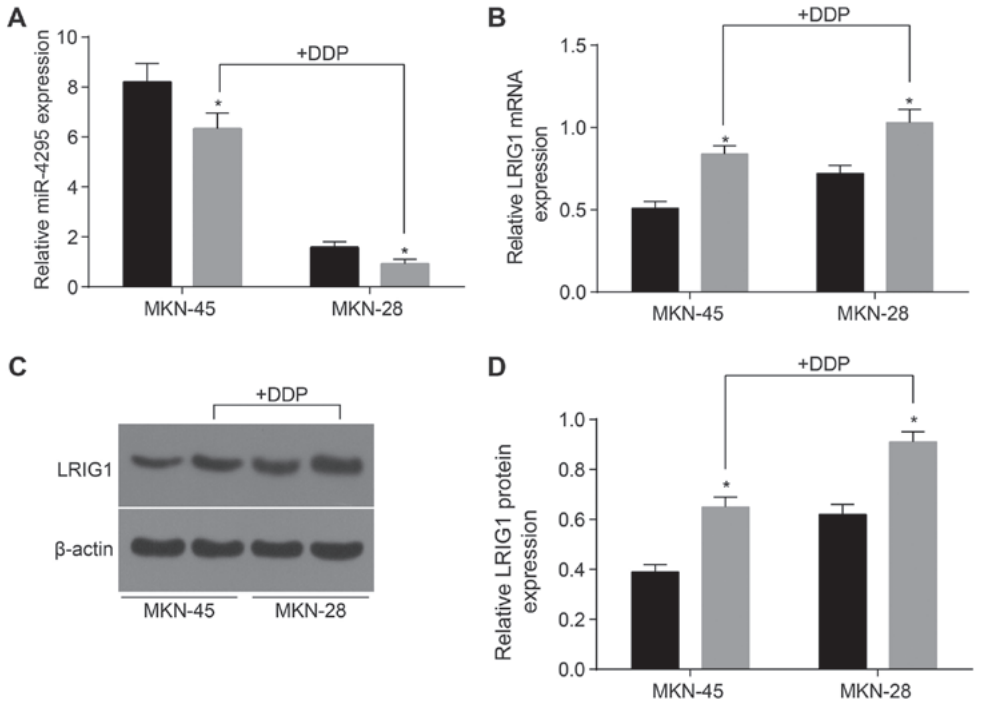

Figure 5. Changes in expression of LRIG1 and miR-4295 in GC cells prior to and following DDP treatment. Panel A, miR-4295 expression prior to and following DDP administration detected by RT-qPCR. Panel B, LRIG1 mRNA expression prior to and following DDP administration detected by RT-qPCR. Panel C and D, protein bands and protein expression of LRIG1 prior to and following DDP administration detected by western blot analysis. *P<0.05 vs. expression prior to DDP administration. LRIG1, leucine-rich repeats and immunoglobulin-like domains 1; miR, microRNA; GC, gastric cancer; DDP, cisplatin; RT-qPCR, reverse transcription-quantitative polymerase chain reaction. Data are presented as the mean ± standard deviation of three independent experiments. Two-tailed Student's t-tests were used to analyze the data.

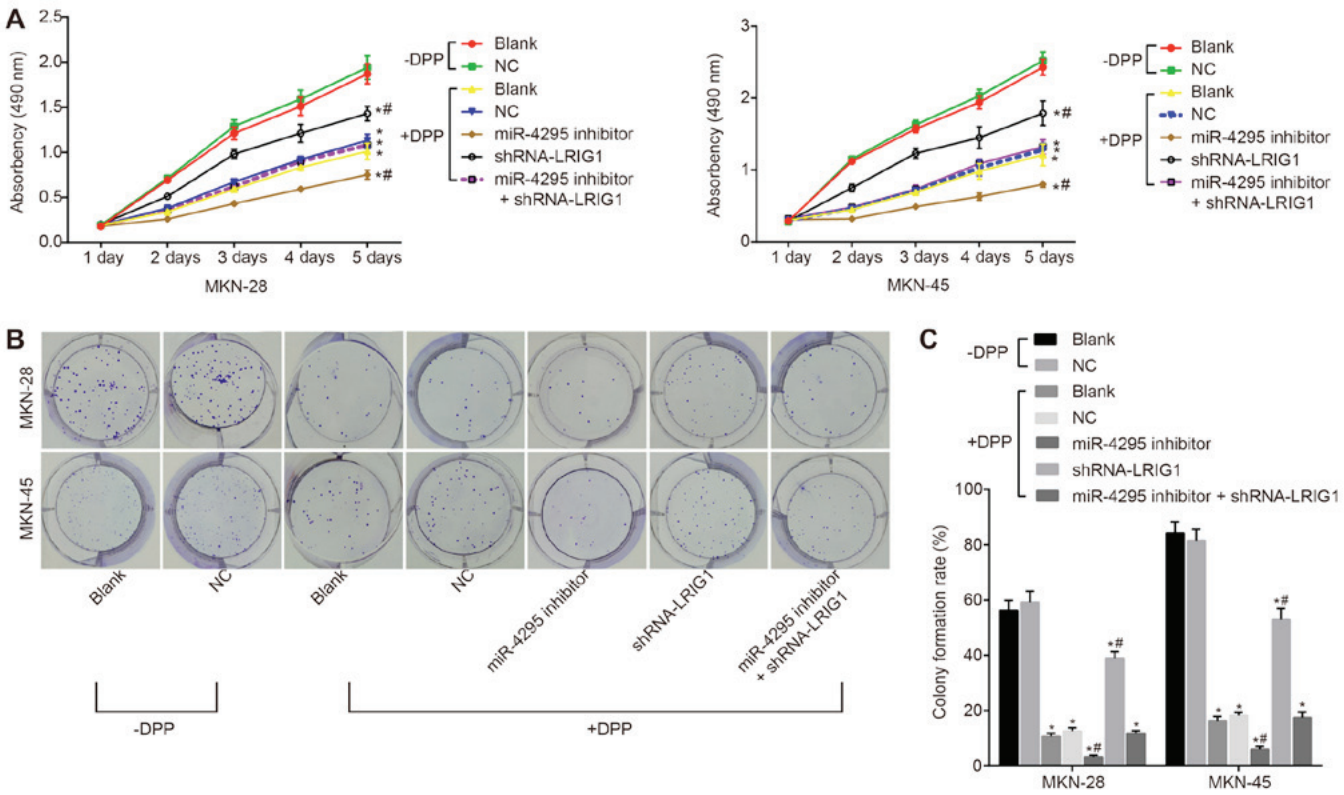

Figure 6. Plate colony formation experiment and MTT assay confirmed that miR-4295 promoted the proliferation of GC cells following transfection. Panel A, cell growth curves of MKN-28 and MKN-45 cell lines detected by MTT assay. Panel B, the plate colony formation experiment in MKN-28 and MKN-45 cell lines. Panel C, cell colony formation rate in MKN-28 and MKN-45 cell lines. *P<0.05 vs. the blank control group without DDP treatment; #P<0.05 vs. the blank control group following DDP treatment. Data are presented as the mean ± standard deviation of three independent experiments. The absorbency comparison was conducted by repeated measurement ANOVA and the cell colony formation rate was determined by one-way ANOVA. miR, microRNA; GC, gastric cancer; DDP, cisplatin; ANOVA, analysis of variance.

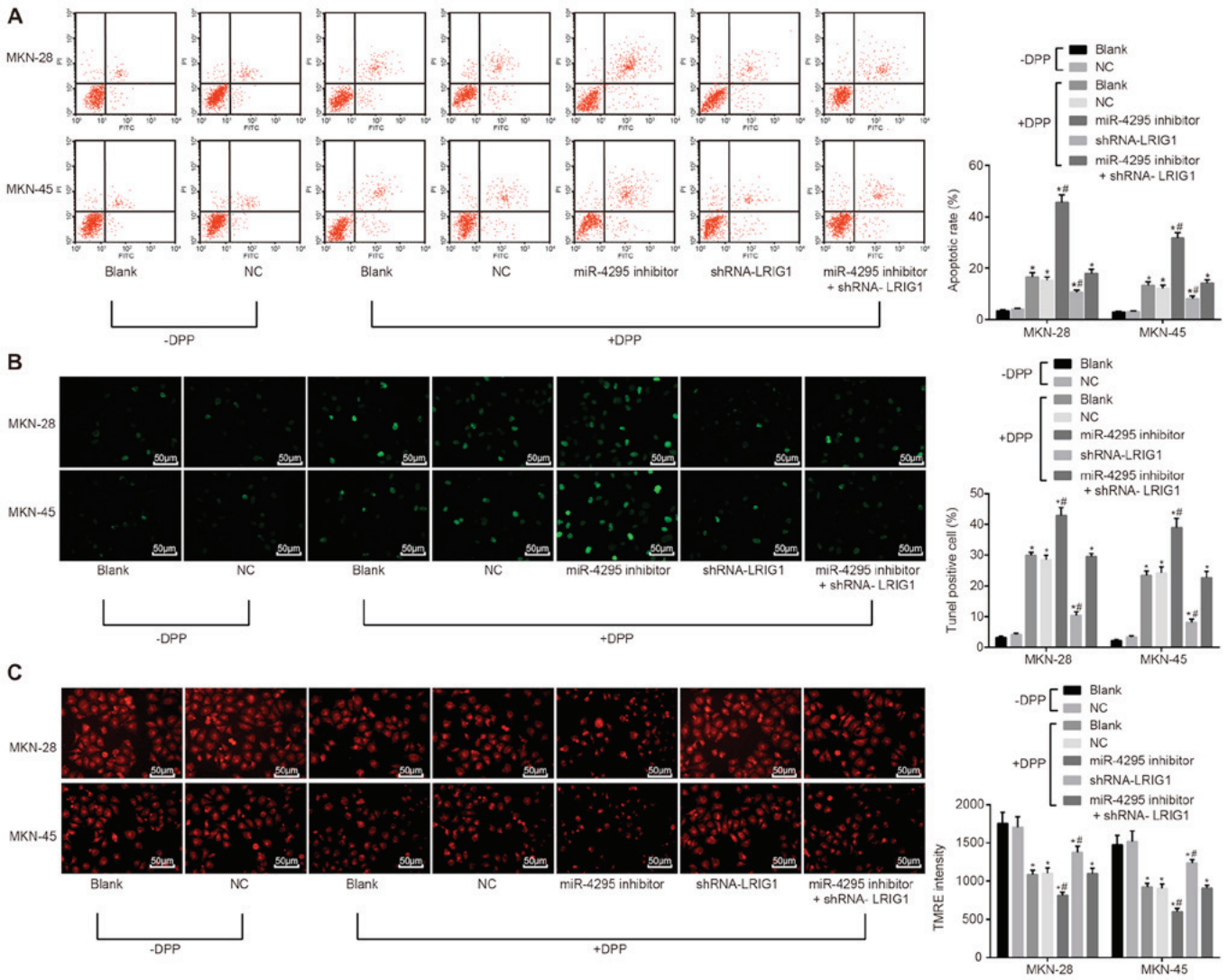

Figure 7. The inhibitory effect of miR-4295 on DDP-induced cell apoptosis in GC cells confirmed by Annexin V-FITC/PI double staining, TUNEL staining and TMRE staining. Panel A, Annexin V-FITC/PI double staining for apoptosis in MKN-28 and MKN-45 cells; Panel B, TUNEL staining for the apoptosis of MKN-28 and MKN-45 cells (x200). Panel C, TMRE staining for mitochondrial transmembrane potential (x200). *P<0.05 vs. the blank control group without DDP treatment; #P<0.05 vs. the blank control group following DDP treatment. Data are presented as the mean ± standard deviation of three independent experiments. miR, microRNA; DDP, cisplatin; GC, gastric cancer; FITC, fluorescein isothiocyanate; PI, propidium iodide; TUNEL, terminal deoxynucleotidyl transferase dUTP nick-end labeling; TMRE, tetramethylrhodamine ethyl ester.

statistically significant difference in the rate of cell apoptosis in the miR-4295 inhibitor + shRNA-LRIG1 co-transfection group, compared with the blank control group.

TMRE staining (Fig. 7C) was used to detect the mitochondrial transmembrane potential. Red fluorescence signal was significantly weakened, transmembrane mitochondrial potential was decreased, and the number of apoptotic cells was increased following DDP treatment, compared with those without DDP treatment (P<0.05). Following DDP treatment, compared with the blank control group, the NC group exhibited no significant differences in the intensity of red fluorescence signal (mitochondria of non-apoptotic cells) and the number of apoptotic cells (P>0.05). Compared with the blank control group, the miR-4295 inhibitor group displayed no red fluorescence signal, decreased the transmembrane potential of mitochondria, and increased the number of apoptotic cells (P<0.05), while the shRNA-LRIG1 exhibited the opposite results (P<0.05). The miR-4295 inhibitor + shRNA-LRIG1 group displayed no significant difference in the number of apoptotic cells, compared with the blank control group (P>0.05). The results indicated that miR-4295 could inhibit the DDP-induced apoptosis of GC cells by targeting LRIG1.

miR-4295 regulates the expression of apoptosis-related genes in DDP-induced GC cells. RT-qPCR and western blot analysis were used to determine the expression of apoptosis-related genes (Fig. 8). Following DDP treatment, compared with the blank control group, the NC group exhibited no significant differences in the mRNA and protein levels of Bcl-2, Bax and Caspase-3 (P>0.05). Compared with the blank control group and the NC group, the shRNA-LRIG1 group exhibited decreased mRNA and protein expression levels of Bax and Caspase-3 (P<0.05), demonstrating that LRIG1 could promote cell apoptosis-related gene expression and activate the cell apoptosis-related signaling pathway. The miR-4295 inhibitor group exhibited increased mRNA and protein expression

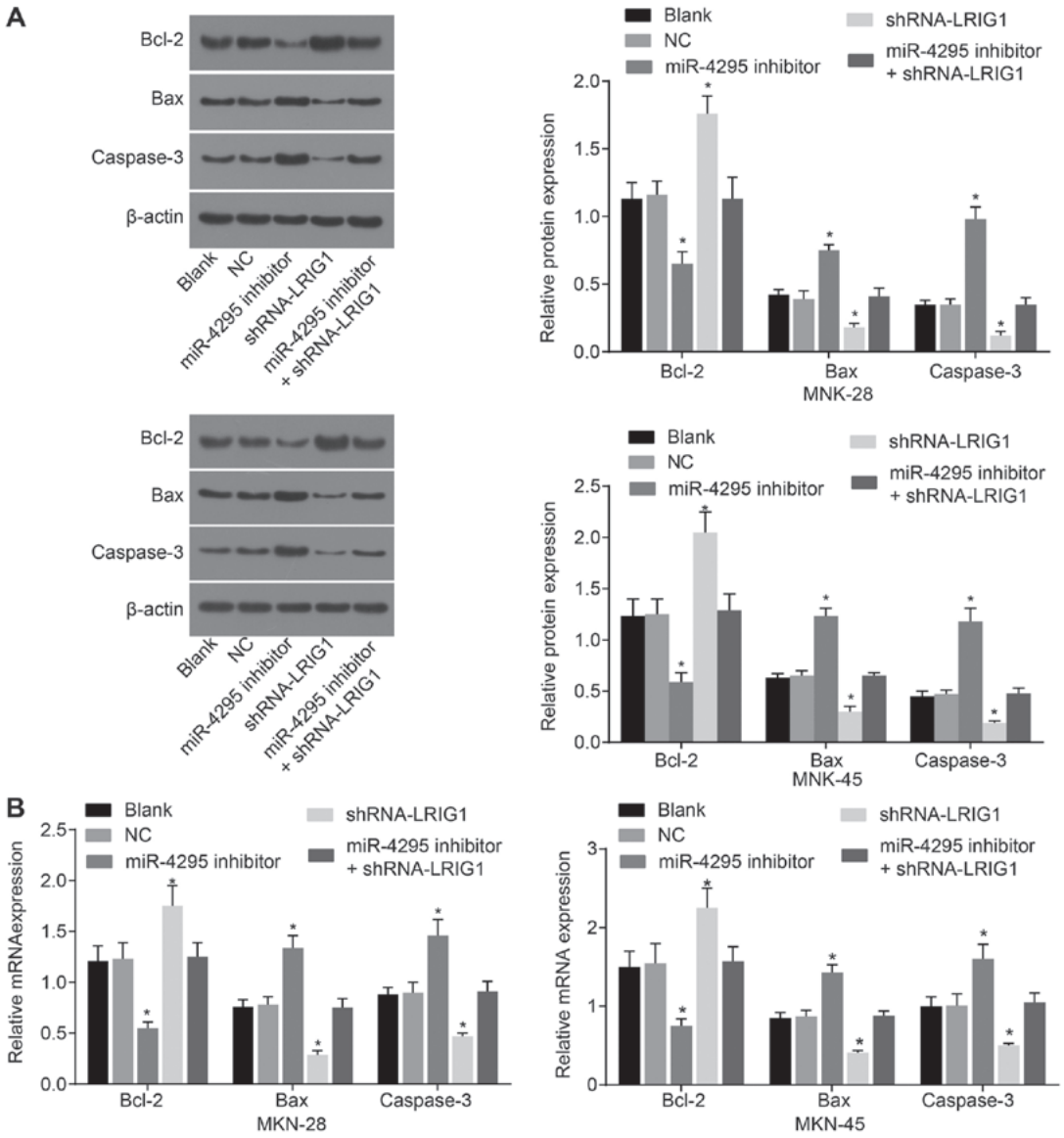

Figure 8. RT-qPCR and western blot analysis demonstrate that miR-4295 mediates apoptosis-related genes in DDP-induced GC cells. Panel A, the protein bands and quantification analysis detected by western blot analysis. Panel B, the quantification analysis for the mRNA expression detected by RT-qPCR. *P<0.05 vs. the blank control group. Data are presented as the mean ± standard deviation of three independent experiments. One-way analysis of variance was used to analyze the data. RT-qPCR, reverse transcription-quantitative polymerase chain reaction; miR, microRNA; GC, gastric cancer; DDP, cisplatin; Bcl-2, B-cell lymphoma 2; Bax, Bcl-2-associated X protein.

levels of Bax and Caspase-3, but decreased expression levels of Bcl-2, compared with the blank control group and the NC group (P<0.05), suggesting that inhibition of miR-4295 may promote DDP-induced GC cell apoptosis. Compared with the blank control group and the NC group, no significant differences in the mRNA and protein expression levels of Bcl-2, Bax and Caspase-3 were observed in the miR-4295 inhibitor + shRNA-LRIG1 group (P>0.05).

miR-4295 promotes activation of the EGFR/PI3K/Akt signaling pathway by targeting LRIG1. RT-qPCR and western blot analysis were used to determine the expression levels of EGFR, PI3K, Akt, p-PI3K and p-Akt. As demonstrated in Fig. 9A, compared with the blank control and NC groups, the protein expression levels of EGFR, PI3K, Akt, p-PI3K and p-Akt were significantly decreased in the miR-4295 inhibitor group (all P<0.05), which indicated that the EGFR/PI3K/Akt signaling pathway was inhibited following DDP treatment. The protein expression levels of EGFR, PI3K, Akt, p-PI3K and p-Akt were increased in the shRNA-LRIG1 group (P<0.05). This result demonstrated that LRIG1 inhibited the activation of the EGFR/PI3K/Akt pathway and induced cell apoptosis. However, there was no statistically significant difference in the mRNA levels of EGFR, PI3K, Akt, p-PI3K and p-Akt in the miR-4295 inhibitor + shRNA-LRIG1 group compared with the blank control and NC groups. Similarly, as demonstrated in Fig. 9B, EGFR, PI3K and Akt mRNA expression was significantly decreased in the miR-4295 inhibitor group compared with the blank control and NC groups (P<0.05), and EGFR, PI3K and Akt mRNA expression was increased in the shRNA-LRIG1 group (P<0.05). There were no statistically significant differences in the EGFR, PI3K and Akt mRNA expression levels in the

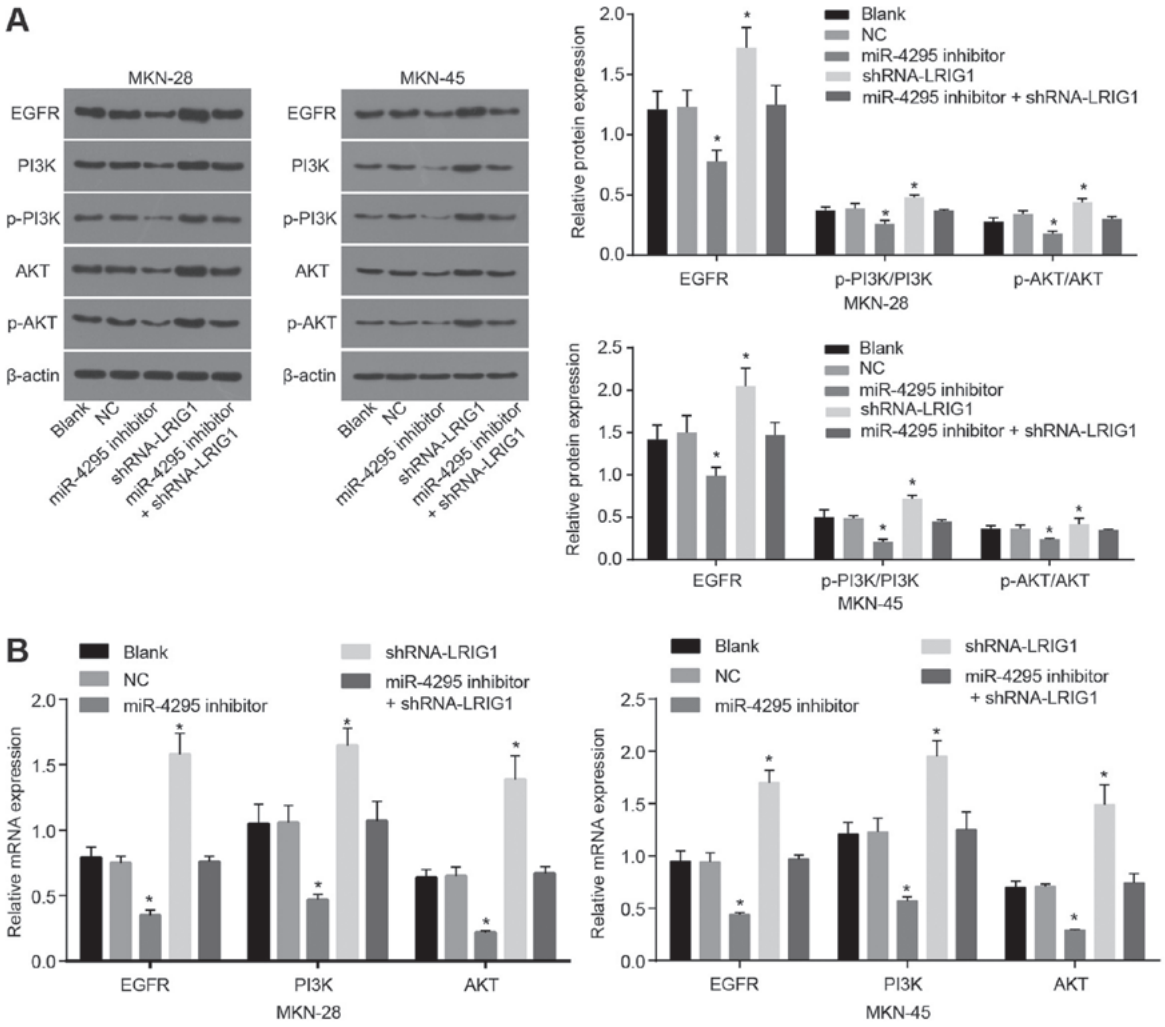

Figure 9. miR-4295 enhances the activation of the EGFR/PI3K/Akt signaling pathway. Panel A, the protein bands and quantification analysis detected by western blot analysis. Panel B, the quantification analysis for the mRNA expression detected by reverse transcription-quantitative polymerase chain reaction. *P<0.05 vs. the blank control group. Data are presented as the mean ± standard deviation of three independent experiments. One-way analysis of variance was used to analyze the data. GC, gastric cancer; EGFR, epidermal growth factor receptor; PI3K, phosphoinositide 3-kinase; Akt, protein kinase B.

miR-4295 inhibitor + shRNA-LRIG1 group, compared with the blank control and NC groups (all P>0.05). The results indicated that miR-4295 promoted the activation of the EGFR/PI3K/Akt signaling pathway by inhibiting LRIG1.

Discussion

GC is regarded as the second most frequent cause of cancer-associated mortality worldwide (28). Recently, microRNAs have become potential targets for GC treatment (29). Therefore, we hypothesized that miR-4295 could inhibit the DDP-induced apoptosis of GC cells without DDP treatment by regulating LRIG1 through activation of the EGFR/PI3K/Akt signaling pathway (Fig. 10).

A significant result of the present study was that miR-4295 was highly expressed in GC cells. Although MKN-28 has been demonstrated to be a contaminated cell line, the misidentification does not affect the results or conclusions of the present study (30). Dysregulation of microRNAs is connected with various cancer sub-types, including GC (31). Overexpression of miR-4295 in glioma tissue was also reported, and its level was revealed to be associated with clinical stage (32). Furthermore, the present study identified that LRIG1 was a downstream target gene of miR-4295, and that LRIG1 was downregulated in GC cells. In the skin and intestine, LRIG1 is a marker of proliferative and quiescent stem cells (33). A recent study reported overexpression of miR-21 in GC and *Helicobacter pylori*-infected gastric mucosa, and the microRNA signature was significantly associated with general mechanisms of GC tumorigenesis (34). The expression of microRNAs is varied in GCs, and specific microRNA signatures characterize histological subtypes. Unique microRNAs are associated with the progression and prognosis of GC (34). The overexpression of miR-4295 significantly increased the proliferation, colony formation and migration of bladder cancer cells (10). Zhang *et al* (13) demonstrated that the suppression of LRIG1 may be mediated by inhibition of the EGFB/PI3K/Akt pathway, and overexpression of LRIG1 in SHG-44 cells inhibited hypoxia-induced activation of the EGFR/PI3K/Akt pathway. MicroRNAs serve a vital role in the pathogenesis of different types of cancer by negatively regulating gene expression at the post-transcriptional level. The results of the study proved that overexpression of miR-4295 aggravated ATC cell proliferation, migration and invasion. MicroRNA expression profiles of

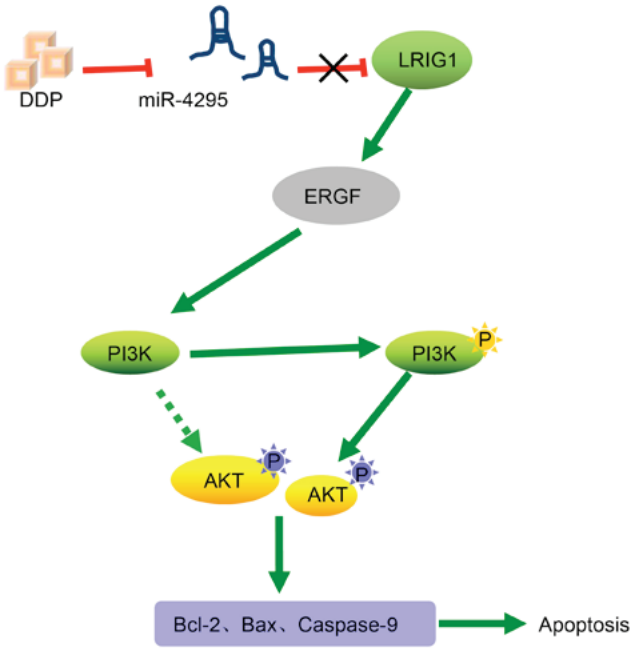

Figure 10. Regulatory mechanisms by which miR-4295 influences the apoptosis in DDP-induced GC cells through activating the EGFR/PI3K/Akt signaling pathway by targeting LRIG1. miR, microRNA; DDP, cisplatin; GC, gastric cancer; EGFR, epidermal growth factor receptor; PI3K, phosphoinositide 3-kinase; Akt, protein kinase B.

malignant disease have offered valuable understanding of the molecular mechanisms underlying carcinogenesis (35). Nan *et al* (9) revealed that miR-4295 was a potential biomarker of cancer diagnosis and therapy.

The data in the present study revealed that DDP induced a reduction in miR-4295 expression and increased LRIG1 expression in GC cells without DDP treatment. DDP is used for malignant disease, including GC, in combination with different antitumor agents. A chemotherapy regimen that includes DDP and MMC is feasible against GC and has potential and possible superiority due to the synergistic interaction of the two agents and the distribution of their toxicity (36). Caspase-3 and survivin regulate apoptosis and were involved in the development of GC (37). miR-1271 exhibited significantly decreased expression in the DDP-resistant GC SGC7901/DDP cell line, and the down-regulation of miR-1271 in SGC7901/DDP cells was followed by the upregulation of insulin-like growth factor 1 receptor/insulin receptor substrate pathway-related proteins (38). Furthermore, the results of the present study implied that miR-4295 promotes the proliferation and inhibits the DDP-induced apoptosis of GC cells. Consistently, it has been demonstrated that overexpression of miR-4295 significantly enhances cell proliferation and suppresses apoptosis in bladder cancer cells (10).

miR-4295 promotes the activation of the EGFR/PI3K/Akt signaling pathway by negatively regulating LRIG1 expression. The EGFR-PI3K-Akt signaling pathway serves an important role in the M. hyorhinis-promoted migration of GC cells, thereby providing a clue to the pathogenesis of M. hyorhinis in GC (39). Stimulation of VEGER2 by VEGF can simultaneously activate several molecular pathways, including the PI3K/Akt mechanistic target of rapamycin signaling pathway. Cell proliferation, migration and survival are mediated by this signaling pathway (40). The role of this pathway in oncogenesis has been widely investigated, and the altered expression or mutation of numerous components of this pathway are involved in human cancer (41). The PI3K/Akt signaling pathway has been firmly established as a vital factor in tumorigenesis (41). PI3K and Akt are important downstream effectors of EGFR, and the EGFR/PI3K/Akt pathway serves an important role in glioma (13). Previous studies presented the central role of PI3K-Akt signaling in several cellular processes involved in cancer, including growth, survival and motility (39).

In conclusion, miR-4295 inhibits the DDP-induced apoptosis of GC cells via the EGFR/PI3K/Akt signaling pathway by targeting the LRIG1 gene. miR-4295 could suppress the apoptosis of GC cells induced by DDP, and LRIG1 could activate the EGFR/PI3K/Akt signaling pathway to induce the apoptosis of GC cells. The novel miR-4295 may provide novel insights into the mechanisms underlying tumor metastasis, and inhibition of miR-4295 may be a potential therapeutic strategy for the treatment of GC in the future.

Acknowledgements

Not applicable.

Funding

The present study was supported by Natural Science Basic Research Project of in Shaanxi Province (grant no. 2015JM8395).

Availability of data and materials

All datasets generated and/or analyzed during the present study are available from the corresponding author on reasonable request.

Authors' contributions

RY, KL and KZ were responsible for the study design; DWY, KZ and CXD were responsible for data collection; RY, HNW and YZ analyzed the data; KL and DWY interpreted the data; RY, KL, HNW and YZ drafted the manuscript; and RY, KL, DWY, HNW, YZ, CXD and KZ approved the final version of the manuscript.

Ethics approval and consent to participate

Not applicable.

Consent for publication

Not applicable.

Competing interests

The authors declare that they have no competing interests.

References

1. Ang TL and Fock KM: Clinical epidemiology of gastric cancer. Singapore Med J 55: 621-628, 2014.

2. Song H, Ekheden IG, Zheng Z, Ericsson J, Nyrén O and Ye W: Incidence of gastric cancer among patients with gastric precancerous lesions: Observational cohort study in a low risk Western population. BMJ 351: h3867, 2015.
3. Chen G, Xu M, Chen J, Hong L, Lin W, Zhao S, Zhang G, Dan G and Liu S: Clinicopathological features and increased expression of toll-like receptor 4 of gastric cardia cancer in a high-risk chinese population. J Immunol Res 2018: 7132868, 2018.
4. He J, Qi H, Chen F and Cao C: MicroRNA-25 contributes to cisplatin resistance in gastric cancer cells by inhibiting forkhead box O3a. Oncol Lett 14: 6097-6102, 2017.
5. Silberman H: Perioperative adjunctive treatment in the management of operable gastric cancer. J Surg Oncol 90: 174-187, 2005.
6. Luo Y, Cui S, Tang F, Shen C, Qi Y, Lu D, Ma L, Yang Y, Li Y, Chen R, *et al*: The combination of crocin with cisplatin suppresses growth of gastric carcinoma cell line BGC-823 and promotes cell apoptosis. Pak J Pharm Sci 30: 1629-1634, 2017.
7. Lai KW, Koh KX, Loh M, Tada K, Subramaniam MM, Lim XY, Vaithilingam A, Salto-Tellez M, Iacopetta B, Ito Y, *et al*; Singapore Gastric Cancer Consortium: MicroRNA-130b regulates the tumour suppressor RUNX3 in gastric cancer. Eur J Cancer 46: 1456-1463, 2010.
8. Xu Y, Zhao F, Wang Z, Song Y, Luo Y, Zhang X, Jiang L, Sun Z, Miao Z and Xu H: MicroRNA-335 acts as a metastasis suppressor in gastric cancer by targeting Bcl-w and specificity protein 1. Oncogene 31: 1398-1407, 2012.
9. Chang L, Guo F, Wang Y, Lv Y, Huo B, Wang L and Liu W: MicroRNA-200c regulates the sensitivity of chemotherapy of gastric cancer SGC7901/DDP cells by directly targeting RhoE. Pathol Oncol Res 20: 93-98, 2014.
10. Nan YH, Wang J, Wang Y, Sun PH, Han YP, Fan L, Wang KC, Shen FJ and Wang WH: MiR-4295 promotes cell growth in bladder cancer by targeting BTG1. Am J Transl Res 8: 4892-4901, 2016.
11. Shao M, Geng Y, Lu P, Xi Y, Wei S, Wang L, Fan Q and Ma W: miR-4295 promotes cell proliferation and invasion in anaplastic thyroid carcinoma via CDKN1A. Biochem Biophys Res Commun 464: 1309-1313, 2015.
12. Jiang J, Yuan Z, Sun Y, Bu Y, Li W and Fei Z: Ginsenoside Rg3 enhances the anti-proliferative activity of erlotinib in pancreatic cancer cell lines by downregulation of EGFR/PI3K/Akt signaling pathway. Biomed Pharmacother 96: 619-625, 2017.
13. Zhang X, Song Q, Wei C and Qu J: LRIG1 inhibits hypoxia-induced vasculogenic mimicry formation via suppression of the EGFR/PI3K/AKT pathway and epithelial-to-mesenchymal transition in human glioma SHG-44 cells. Cell Stress Chaperones 20: 631-641, 2015.
14. Wang B, Jiang H, Wang L, Chen X, Wu K, Zhang S, Ma S and Xia B: Increased MIR31HG lncRNA expression increases gefitinib resistance in non-small cell lung cancer cell lines through the EGFR/PI3K/AKT signaling pathway. Oncol Lett 13: 3494-3500, 2017.
15. Han BH, Lee YJ, Yoon JJ, Choi ES, Namgung S, Jin XJ, Jeong DH, Kang DG and Lee HS: Hwangryunhaedoktang exerts anti-inflammation on LPS-induced NO production by suppressing MAPK and NF-κB activation in RAW264.7 macrophages. J Integr Med 15: 326-336, 2017.
16. Jiang Q, Wu C and Zhang Q: microRNA-34a participates in lipopolysaccharide mediated sepsis related renal function impairment via Kruppel-like factor 4. Zhonghua Wei Zhong Bing Ji Jiu Yi Xue 30: 351-354, 2018 (In Chinese).
17. Mondal J, Samadder A and Khuda-Bukhsh AR: Psorinum 6x triggers apoptosis signals in human lung cancer cells. J Integr Med 14: 143-153, 2016.
18. Cimas FJ, Callejas-Valera JL, Pascual-Serra R, García-Cano J, Garcia-Gil E, De la Cruz-Morcillo MA, Ortega-Muelas M, Serrano-Oviedo L, Gutkind JS and Sánchez-Prieto R: MKP1 mediates chemosensitizer effects of E1a in response to cisplatin in non-small cell lung carcinoma cells. Oncotarget 6: 44095-44107, 2015.
19. Kang Y, Nagaraja AS, Armaiz-Pena GN, Dorniak PL, Hu W, Rupaimoole R, Liu T, Gharpure KM, Previs RA, Hansen JM, *et al*: Adrenergic Stimulation of DUSP1 Impairs Chemotherapy Response in Ovarian Cancer. Clin Cancer Res 22: 1713-1724, 2016.
20. Cortes-Sempere M, Chattopadhyay S, Rovira A, Rodriguez-Fanjul V, Belda-Iniesta C, Tapia M, Cejas P, Machado-Pinilla R, Manguan-García C, Sánchez-Pérez I, *et al*: MKP1 repression is required for the chemosensitizing effects of NF-kappaB and PI3K inhibitors to cisplatin in non-small cell lung cancer. Cancer Lett 286: 206-216, 2009.
21. Wang Q, Shi S, He W, Padilla MT, Zhang L, Wang X, Zhang B and Lin Y: Retaining MKP1 expression and attenuating JNK-mediated apoptosis by RIP1 for cisplatin resistance through miR-940 inhibition. Oncotarget 5: 1304-1314, 2014.
22. Wang X, Xiao Q, Xing X, Tian C, Zhang H, Ye F, Wan F, Wang B, Guo D and Lei T: LRIG1 enhances cisplatin sensitivity of glioma cell lines. Oncol Res 20: 205-211, 2012.
23. Cao W, Yang W, Fan R, Li H, Jiang J, Geng M, Jin Y and Wu Y: miR-34a regulates cisplatin-induce gastric cancer cell death by modulating PI3K/AKT/survivin pathway. Tumour Biol 35: 1287-1295, 2014.
24. Cheng C, Qin Y, Zhi Q, Wang J and Qin C: Knockdown of long non-coding RNA HOTAIR inhibits cisplatin resistance of gastric cancer cells through inhibiting the PI3K/Akt and Wnt/β-catenin signaling pathways by up-regulating miR-34a. Int J Biol Macromol 107: 2620-2629, 2018.
25. Hu B, Zhang H, Wang Z, Zhang F, Wei H and Li L: LncRNA CCAT1/miR-130a-3p axis increases cisplatin resistance in non-small-cell lung cancer cell line by targeting SOX4. Cancer Biol Ther 18: 974-983, 2017.
26. Li N, Yang L, Wang H, Yi T, Jia X, Chen C and Xu P: MiR-130a and MiR-374a function as novel regulators of cisplatin resistance in human ovarian cancer A2780 cells. PLoS One 10: e0128886, 2015.
27. Li NW, Wang HJ, Yang LY, Jia XB, Chen C and Wang X: Regulatory effects and associated mechanisms of miR-130a molecules on cisplatin resistance in ovarian cancer A2780 cell lines. Sichuan Da Xue Xue Bao Yi Xue Ban 44: 865-870, 2013 (In Chinese).
28. Łukaszewicz-Zając M, Szmitkowski M, Litman-Zawadzka A and Mroczko B: Matrix metalloproteinases and their tissue inhibitors in comparison to other inflammatory proteins in gastric cancer (GC). Cancer Invest 34: 305-312, 2016.
29. Wang H, Jiang Z, Chen H, Wu X, Xiang J and Peng J: MicroRNA-495 inhibits gastric cancer cell migration and invasion possibly via targeting high mobility group AT-Hook 2 (HMGA2). Med Sci Monit 23: 640-648, 2017.
30. Capes-Davis A, Theodosopoulos G, Atkin I, Drexler HG, Kohara A, MacLeod RA, Masters JR, Nakamura Y, Reid YA, Reddel RR, *et al*: Check your cultures! A list of cross-contaminated or misidentified cell lines. Int J Cancer 127: 1-8, 2010.
31. Mraz M and Pospisilova S: MicroRNAs in chronic lymphocytic leukemia: From causality to associations and back. Expert Rev Hematol 5: 579-581, 2012.
32. Li X, Zheng J, Diao H and Liu Y: RUNX3 is down-regulated in glioma by Myc-regulated miR-4295. J Cell Mol Med 20: 518-525, 2016.
33. Choi E, Lantz TL, Vlacich G, Keeley TM, Samuelson LC, Coffey RJ, Goldenring JR and Powell AE: Lrig1^{+} gastric isthmal progenitor cells restore normal gastric lineage cells during damage recovery in adult mouse stomach. Gut 67: 1595-1605, 2018.
34. Ueda T, Volinia S, Okumura H, Shimizu M, Taccioli C, Rossi S, Alder H, Liu CG, Oue N, Yasui W, *et al*: Relation between microRNA expression and progression and prognosis of gastric cancer: A microRNA expression analysis. Lancet Oncol 11: 136-146, 2010.
35. Miao J, Wu S, Peng Z, Tania M and Zhang C: MicroRNAs in osteosarcoma: Diagnostic and therapeutic aspects. Tumour Biol 34: 2093-2098, 2013.
36. Saikawa Y, Kubota T, Kuo TH, Kase S, Furukawa T, Tanino H, Ishibiki K and Kitajima M: Synergistic antitumor activity of mitomycin C and cisplatin against gastric cancer cells in vitro. J Surg Oncol 54: 98-102, 1993.
37. Kania J, Konturek SJ, Marlicz K, Hahn EG and Konturek PC: Expression of survivin and caspase-3 in gastric cancer. Dig Dis Sci 48: 266-271, 2003.
38. Yang M, Shan X, Zhou X, Qiu T, Zhu W, Ding Y, Shu Y and Liu P: miR-1271 regulates cisplatin resistance of human gastric cancer cell lines by targeting IGF1R, IRS1, mTOR, and BCL2. Anticancer Agents Med Chem 14: 884-891, 2014.
39. Duan H, Qu L and Shou C: Activation of EGFR-PI3K-AKT signaling is required for Mycoplasma hyorhinis-promoted gastric cancer cell migration. Cancer Cell Int 14: 135, 2014.
40. Zhang W, Tan Y and Ma H: Combined aspirin and apatinib treatment suppresses gastric cancer cell proliferation. Oncol Lett 14: 5409-5417, 2017.
41. Luo J, Manning BD and Cantley LC: Targeting the PI3K-Akt pathway in human cancer: Rationale and promise. Cancer Cell 4: 257-262, 2003.